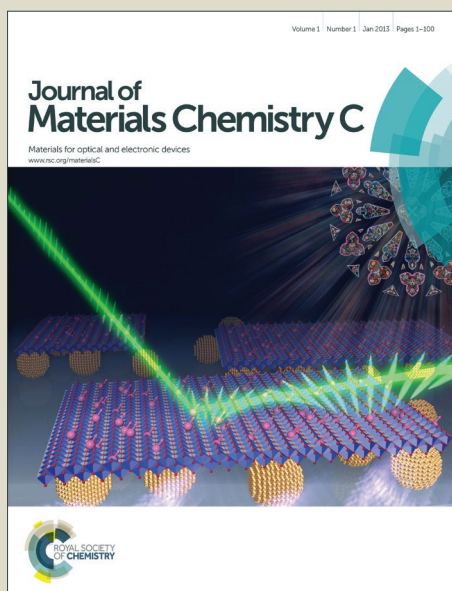


# Journal of Materials Chemistry C

Accepted Manuscript



This article can be cited before page numbers have been issued, to do this please use: B. Pradhan, S. K. Pathak, R. K. Gupta, M. Gupta, S. K. PAL and A. Ammathnadu Sudhakar, *J. Mater. Chem. C*, 2016, DOI: 10.1039/C6TC01260D.



This is an *Accepted Manuscript*, which has been through the Royal Society of Chemistry peer review process and has been accepted for publication.

*Accepted Manuscripts* are published online shortly after acceptance, before technical editing, formatting and proof reading. Using this free service, authors can make their results available to the community, in citable form, before we publish the edited article. We will replace this *Accepted Manuscript* with the edited and formatted *Advance Article* as soon as it is available.

You can find more information about *Accepted Manuscripts* in the [Information for Authors](#).

Please note that technical editing may introduce minor changes to the text and/or graphics, which may alter content. The journal's standard [Terms & Conditions](#) and the [Ethical guidelines](#) still apply. In no event shall the Royal Society of Chemistry be held responsible for any errors or omissions in this *Accepted Manuscript* or any consequences arising from the use of any information it contains.

# Star-shaped Fluorescent Liquid Crystals derived from *s*-triazine and 1,3,4-oxadiazole moieties

Balaram Pradhan<sup>a</sup>, Suraj Kumar Pathak<sup>a</sup>, Ravindra Kumar Gupta<sup>a</sup>, Monika Gupta<sup>b</sup>, Santanu Kumar Pal<sup>b</sup> and Ammathnadu S.Achalkumar<sup>a\*</sup>

<sup>a</sup>*Department of Chemistry,  
Indian Institute of Technology Guwahati, Guwahati, 781039, Assam, India.*

<sup>b</sup>*Indian Institute of Science Education and Research, Mohali, Sector-81,  
Knowledge City, Manauli 140306, Punjab, India.*

**Abstract:** Star-shaped molecules with a central triazine core appended with three 1,3,4-oxadiazole arms have been designed with the variation in the number, length and pattern of peripheral chain substitution. These compounds were investigated for their thermal, electrochemical and photophysical behavior. These nonconventional molecules stabilized wide range columnar phases and demonstrated how one can tune the liquid crystal self-assembly through simple structural modification. The photophysical properties of these star shaped molecules are extremely dependent on the number and pattern of peripheral chain substitution. These compounds exhibit blue and green luminescence in solid/liquid crystal state. The ability to overcome aggregation induced quenching is due to the favorable packing of these molecules in solid state. These solid-state emissive materials with good thermal stability, lower band gap may find application in the construction of emissive displays and organic lasers.

## Introduction

The last four decades have witnessed tremendous research activities with respect to design and synthesis of various discotic liquid crystals.<sup>1</sup> Discotic liquid crystals are designed with the general structural template where a central disc-like core is substituted with three or more flexible chains. Discotic Liquid crystals mainly stabilize two mesophases *viz.* columnar (Col) phase and nematic (N) phase. Columnar phase formed by the one-dimensional stacking of discs to form columns. Based on the arrangement of these columns into different lattices they are classified into different columnar phases. Nematic phase is formed by the organization of discs with long-range orientational order but with no positional order. Over the years several innovative nonconventional molecular designs were shown to stabilize Col phases, which were initially observed for disc shaped molecules. These classes are polycatenars, dendrimers, metallomesogens, bent shaped molecules, oligomers, polymers and star shaped molecules.<sup>2</sup> Star shaped mesogens or 'hekates' are relatively a new class of nonconventional molecules that stabilize columnar liquid crystalline phases. These molecules are formed by the covalent linking

of three arms symmetrically to a central core.<sup>3</sup> These arms may be linked to the central core through flexible or semi flexible or rigid linkers. Shape persistent star shaped mesogens are obtained, when the linkers connecting central core and three arms are rigid. These molecules lack the shape anisotropy of discotics required to exhibit mesophases, but their ability to form mesophases is solely driven by the nanophase segregation of chemically or physically different molecular subunits and their tendency to fill the space efficiently in bulk. Advantage of this molecular design with respect to discotics is, the synthetic flexibility provided to incorporate various functional units into the molecular structure. Hekates or star shaped mesogens can exhibit a variety of phases like nematic, columnar, cubic or soft crystal phases, because of the peculiar structure and the ease of tunability associated with this molecular design. The presence of the voids between the arms of the molecular structure helps the mesophases to freeze in glassy state. Several 1,3,5-substituted benzene based or heterocyclic cores have been utilized to prepare these star shaped mesogens. *s*-1,3,5-Triazine is a readily available  $C_3$ -symmetrical, trifunctional core to prepare star shaped mesogens.<sup>4</sup> Being a  $C_3$ -symmetric planar central core which helps in the self-assembly, it also acts as a *n*-type semiconductor owing to its electron poor nature. Triazine core can also be employed as a H-bonding acceptor, which stabilize supramolecular liquid crystalline self-assembly.<sup>5</sup> Triazine based central core is also used in the synthesis of oligomers<sup>6</sup> and dendrimers.<sup>7</sup> This core has also been utilized in the construction of octupolar materials<sup>8</sup> which show nonlinear optical activity with large first hyperpolarizability. 1,3,5-Triazine based star shaped mesogens have been prepared by one of the following methods, (i) the reaction of nucleophilic group functionalized aromatics with cyanuril chloride<sup>9</sup>; (ii) nucleophilic<sup>9</sup> or palladium catalyzed substitutions<sup>10</sup> with trihalo-1,3,5-triazines and (iii) cyclotrimerization of nitriles.<sup>11, 12b, 17</sup> Many fluorophores like styrene,<sup>9,12</sup> toluene,<sup>13</sup> carbazole<sup>14</sup> and triazole<sup>15</sup> and thiophenes<sup>16</sup> are connected to this central 1,3,5-triazine core to obtain luminescent mesogens. Marder *et.al.* prepared triazine derivatives, where three trialkoxy phenyl substituted 1,3,4-oxadiazole moieties are directly connected to the central triazine cores.<sup>18</sup> Incorporation of 1,3,4-oxadiazoles in to the molecular structure has some advantages, as 1,3,4-oxadiazoles are well-known for their stability towards thermal, hydrolytic and oxidative degradation, intense fluorescence and good electron transporting properties. These compounds are widely used as electron carrier/hole blocking materials and also as electroluminescent layers in organic light emitting devices. Many other research groups have prepared star shaped molecules containing oxadiazole moieties connected to central benzene core at 1,3 and 5-positions.<sup>18, 19</sup> In comparison

to these benzene based hecates, reports on the triazine based hecates with 1,3,4-oxadiazole moieties are scarce. Probably the associated increase in the melting points with the incorporation of heterocycles discouraged the researchers. In this communication we present hitherto unreported fluorescent triazine based hecates with three unsymmetrically substituted 1,3,4-oxadiazole moieties, which stabilize wide range columnar hexagonal phase. The synthesized compounds vary from each other with respect to the number and length of the flexible chains. The number and length of the peripheral tails have a significant effect on the type and range of the Col phase. Lower chain length usually enhances the core-core interaction, which leads to the stabilization of columnar rectangular (Col<sub>r</sub>) phase, while the higher chain length usually promote columnar hexagonal (Col<sub>h</sub>) phase.<sup>1d</sup> We are attempting to shed light on the structure property relations in this class of star shaped molecules with respect to their thermal behavior and photophysical properties.

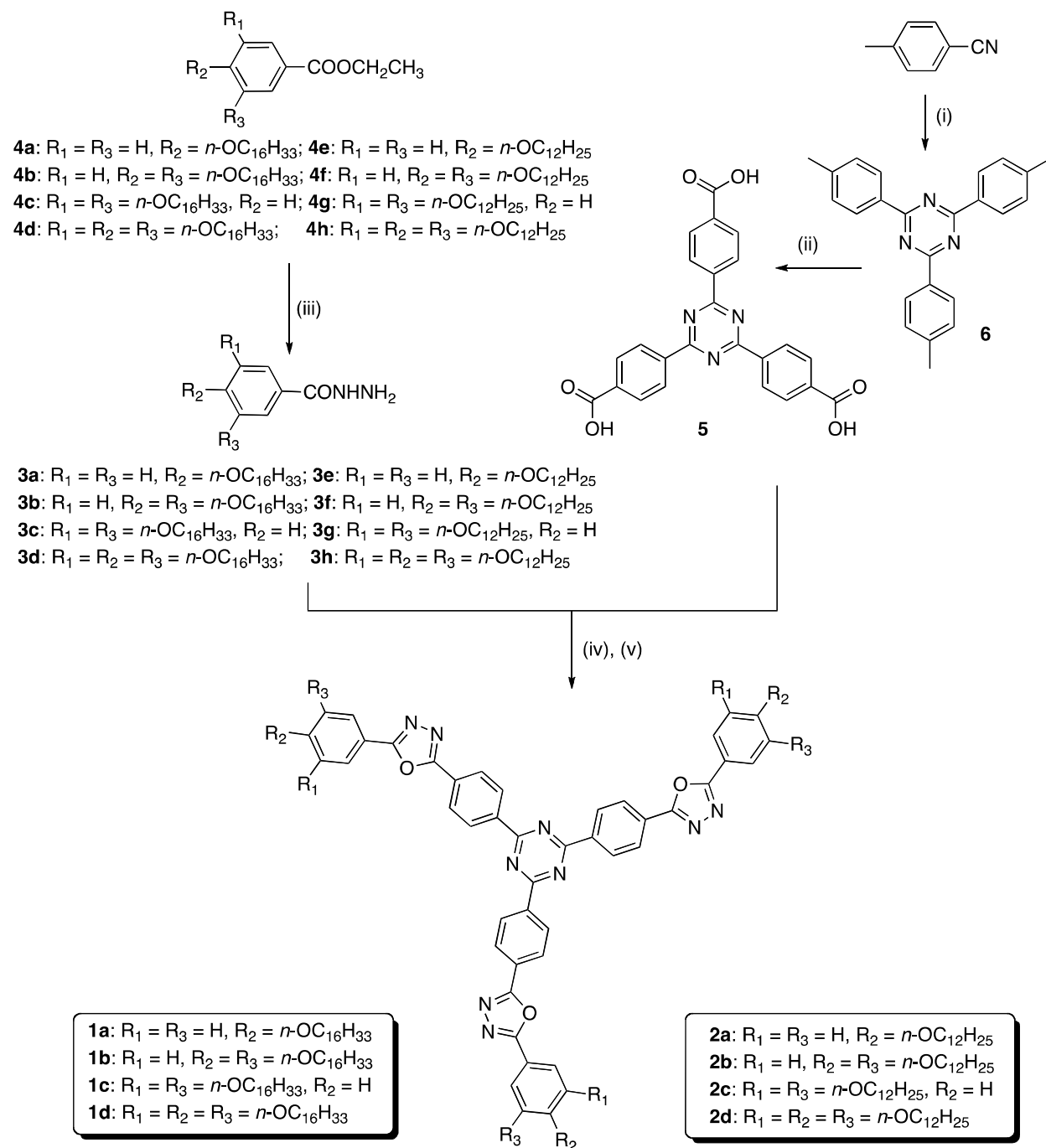
## Results and discussion

**Synthesis and Characterization.** The synthetic strategy to obtain the target molecules and their precursors is illustrated in scheme 1. General procedures for the syntheses of ethyl gallate, 3,4-hexadecyloxy or 3,4-dodecyloxy ethyl benzoate, 3,5-hexadecyloxy ethyl benzoate, 3,5-dodecyloxy ethyl benzoate, 3,4,5-hexadecyloxy ethyl gallate,<sup>20</sup> 3,4,5-dodecyloxy ethyl gallate,<sup>20</sup> 4-hexadecyloxy ethyl benzoate<sup>21</sup> and 4-dodecyloxy ethyl benzoate<sup>21</sup> are reported earlier. Alkoxy esters (**4a-h**) were transformed to their respective hydrazides (**3a-h**) by treating with hydrazine hydrate in ethanol or *n*-butanol as solvent.<sup>19,22</sup> Hydrazides **3a-h** on refluxing with 4,4',4''-(1,3,5-triazine-2,4,6-triyl)tribenzoic acid chloride in THF in presence of triethylamine yielded tri-*N*-benzoylbenzohydrazides.<sup>19</sup> These compounds were heated with POCl<sub>3</sub> to obtain the target molecules **1a-d** and **2a-d**.<sup>19,22</sup> The key intermediate 4,4',4''-(1,3,5-triazine-2,4,6-triyl)tribenzoic acid (**5**) was prepared by chromic oxide mediated oxidation of 2,4,6-tri-*p*-tolyl-1,3,5-triazine (**6**) in good yield.<sup>23</sup> Compound **6** was in turn obtained by the triflic acid catalyzed trimerization of *p*-tolunitrile.<sup>24</sup> The structures of all the intermediates and target molecules were confirmed using <sup>1</sup>H NMR, <sup>13</sup>C NMR, IR spectroscopy and MALDI-TOF mass spectra. (See the supporting information (SI) for the details).

**Thermal behavior.** All the compounds were investigated with the help of Polarizing Optical Microscopy (POM) and Differential Scanning Calorimetry (DSC). Mesomorphic behavior, phase

transition temperatures and associated enthalpy changes are presented in table 1. Figure 1 graphically represents the thermal behavior of compounds **1a-d** and **2a-d** in first cooling cycle.

### Scheme 1. Synthesis of star shaped LCs.<sup>a</sup>



<sup>a</sup>(i)  $\text{CF}_3\text{SO}_3\text{H}$ , dry DCM, 0 °C-rt, 12 h, 90%; (ii)  $\text{CH}_3\text{COOH}$ ,  $\text{H}_2\text{SO}_4$ ,  $\text{CrO}_3$ ,  $\text{Ac}_2\text{O}$ , 0 °C-rt, 24 h, 85%; (iii)  $\text{NH}_2\text{NH}_2 \cdot \text{H}_2\text{O}$ , ethanol, reflux, 48 h (65–75%); (iv) 4,4',4''-s-triazine-2,4,6-triyl-tribenzoic acid chloride, THF, triethylamine, 6 h, reflux; (v)  $\text{POCl}_3$ , reflux, 17 h (45–50%).

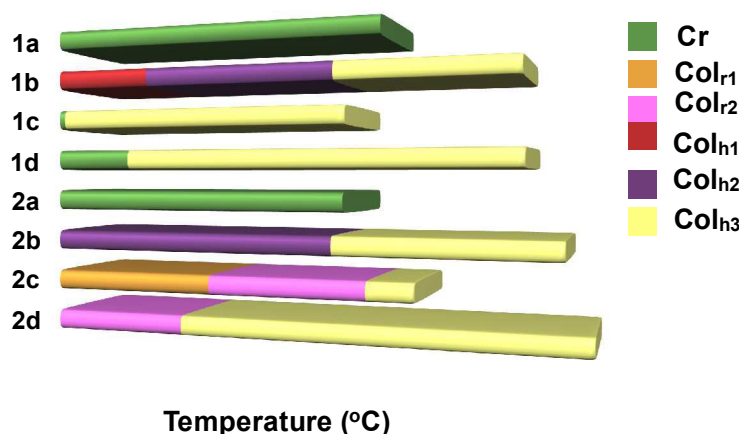


**Figure 1.** Bargraph summarizing the thermal behavior of compounds **1a-d** and **2a-d** (first cooling cycle)

**Table 1.** Phase transition temperatures<sup>a</sup> (°C) and corresponding enthalpies (kJ/mol) of hekates.

Entry	Phase sequence	
	2 <sup>nd</sup> Heating	1 <sup>st</sup> Cooling
<b>1a</b>	Cr 175.4 (3) I	I 172.4 (2.4) Cr
<b>1b</b>	Col <sub>h1</sub> 53.4 (106.3) Col <sub>h2</sub> 152.5 (80.6) Col <sub>h3</sub> 238.5 (18.4) I	I 237.1 (17.2) Col <sub>h3</sub> 149 (80.2) Col <sub>h2</sub> 50.37 (207.1) Col <sub>h1</sub>
<b>1c</b>	Cr 5.4 (127.4) Col <sub>h</sub> 156.8 (9.9) I	I 154.6 (11.1) Col <sub>h</sub> 3 (173.7) Cr
<b>1d</b>	Cr 47.4 (163.8) Col <sub>h</sub> 240 (34.1) I	I 238.1 (31.7) Col <sub>h</sub> 39.9 (526.8) Cr
<b>2a</b>	Cr <sub>1</sub> 53.6 (17.2) Cr <sub>2</sub> 157.7 (126.1) I	I 154.1 (9.5) Cr <sub>2</sub> 41.4 (20.8) Cr <sub>1</sub>
<b>2b</b>	Cr 48.8 (225.03) Col <sub>h1</sub> 161.1 (69.1) Col <sub>h2</sub> 251.2 (14.7) I	I 255.3 (14.0) Col <sub>h2</sub> 148.1 (59.9) Col <sub>h1</sub> <sup>b</sup>
<b>2c</b>	Cr 48.9 (382.04) Col <sub>r1</sub> <sup>c</sup> 90 Col <sub>r2</sub> 170 Col <sub>h</sub> 190.1 (22.3) I	I 188.1 (20.9) Col <sub>h</sub> <sup>c</sup> 165 Col <sub>r2</sub> 84.9 (25.3) Col <sub>r1</sub> <sup>b</sup>
<b>2d</b>	Col <sub>r</sub> 86.6 (135.2) Col <sub>h</sub> 276.38 (24.8) I	I 267.9 (429.0) Col <sub>h</sub> 69.7 (26.32) Col <sub>r</sub> <sup>b</sup>

<sup>a</sup>Peak temperatures in the DSC thermograms obtained during the first heating and cooling cycles at 5 °C/min. Col<sub>h</sub> = Columnar hexagonal phase; <sup>b</sup>Mesophase freezing in the glassy state; <sup>c</sup> Transition detected in polarizing optical microscope but not observed in DSC.

Compound **1a** with three hexadecyloxy tails did not show any mesophase and showed a crystal to isotropic transition at 173 °C. It did not show any mesophase on cooling cycle, instead an isotropic to crystal transition at 172 °C. This shows that three flexible tails are not enough to induce the nanophase segregation of molecular subunits in this class of star shaped molecules.<sup>25</sup> POM images of this compound at different temperatures indicated the crystalline nature of the sample (Fig. S53e and f). This was surprising considering a small enthalpy change ( $\Delta H = 2-3$  kJ/mol) observed in DSC thermograms (in heating and cooling cycles).

Compound **1b** with six hexadecyloxy tails exhibited enantiotropic mesomorphic behavior. In the heating cycle the compound showed a crystal to mesophase transition ( $\Delta H = 104.2$  kJ/mol) at a temperature of  $\approx 52$  °C. This birefringent liquid undergoes further transition at  $\approx 153$ °C as observed in DSC scans (See SI), before going to an isotropic liquid state at 239 °C. On cooling the isotropic liquid a dendritic growth was appeared which soon coalesces in to a mosaic pattern interspersed with homeotropic regions (Fig.2a). At 149 °C a transition was

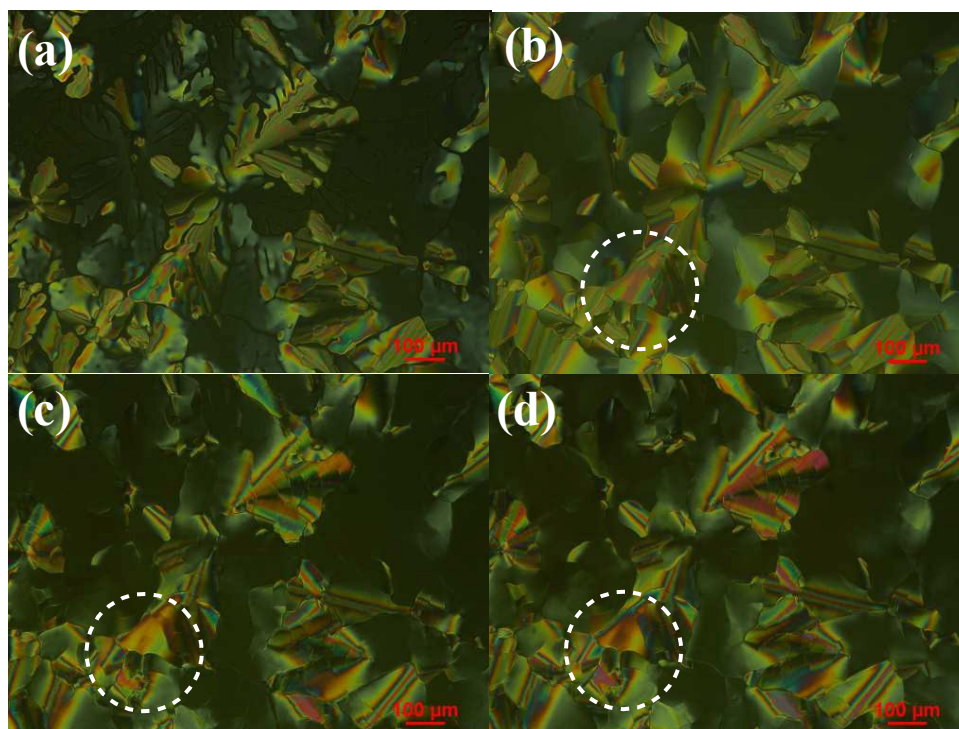


**Figure 2.** Photomicrographs of textures as seen by POM for the  $Col_{h3}$  phase of compound **1b** (a) at 230 °C; (b)  $Col_{h3}$  phase at 155 °C; (c)  $Col_{h2}$  phase at 134 °C; (d)  $Col_{h1}$  phase at 28 °C.

observed in the mesophase, where the texture remains same, but the color of the mosaic pattern gets changed (Fig.2b-c). On further cooling a broad exothermic peak ( $\Delta H = 207.1$  kJ/mol) corresponding to crystallization was observed in the DSC scan at  $\approx 50$ °C, while the texture remains unchanged with a concurrent loss of fluidity (Fig. 3a and 2d). In the next heating scan a transition appeared at a temperature of  $\approx 53$ °C ( $\Delta H = 106.3$ kJ/mol) showing that this transition is not due to glass forming.

In order to assign the symmetry of the columnar phase powder X-ray diffraction of the sample was carried out at different temperature intervals. X-ray diffraction of the sample carried out at 200 °C showed a sharp peak centered at 43.2 Å at the low-angle region, followed by two diffused peaks at 5.18 Å and 3.76 Å respectively (Fig. 3b, Table 2).

**Table 2.** Results of (*hkl*) indexation of XRD profiles of the compounds at a given temperature (T) of mesophase

Compounds ( <i>D</i> /Å)	Phase ( <i>T</i> /°C)	<i>d</i> <sub>obs</sub> (Å)	<i>d</i> <sub>cal</sub> (Å)	Miller indices <i>hkl</i>	Lattice parameter (Å)
<b>1b</b> (65.78)	Col <sub>h3</sub> (200)	43.2 5.18 ( <i>h<sub>a</sub></i> ) 3.76 ( <i>h<sub>c</sub></i> )	43.20	100 001	<i>a</i> = 49.89
	Col <sub>h2</sub> (100)	45.37 4.96 ( <i>h<sub>a</sub></i> ) 3.74 ( <i>h<sub>c</sub></i> )	45.37	100 001	<i>a</i> = 52.36
	Col <sub>h1</sub> (25)	45.34 4.68 ( <i>h<sub>a</sub></i> ) 3.63 ( <i>h<sub>c</sub></i> )	45.33	100 001	<i>a</i> = 52.35
<b>1c</b> (64.31)	Col <sub>h</sub> (140)	39.54 5.11 ( <i>h<sub>a</sub></i> ) 3.77 ( <i>h<sub>c</sub></i> )	39.51	100 001	<i>a</i> = 45.63
	Col <sub>h</sub> (100)	39.56 5.07 ( <i>h<sub>a</sub></i> ) 3.76 ( <i>h<sub>c</sub></i> )	39.53	100 001	<i>a</i> = 45.65
	Col <sub>h</sub> (25)	39.59 4.88 ( <i>h<sub>a</sub></i> ) 3.78 ( <i>h<sub>c</sub></i> )	39.56	100 001	<i>a</i> = 45.69
<b>1d</b> (66.46)	Col <sub>h</sub> (200)	41.33 23.04 16.06 5.20 ( <i>h<sub>a</sub></i> ) 3.82 ( <i>h<sub>c</sub></i> )	41.32 23.86 15.62	100 110 210 001	<i>a</i> = 47.72
	Col <sub>h</sub> (150)	41.32 23.51 15.89 5.12 ( <i>h<sub>a</sub></i> ) 3.76 ( <i>h<sub>c</sub></i> )	41.29 23.84 15.60	100 110 210 001	<i>a</i> = 47.68

Though the observation of a single peak at low angle does not unambiguously confirm the Col<sub>h</sub> phase, textural evidence strongly suggests that it is Col<sub>h</sub> phase. The absence of other peaks in low angle is generally ascribed to a minimum in the form factor and reported earlier.<sup>22,26</sup> The sharp peak at the low angle specifies the distance between the adjacent(100) planes, *i.e.* *d*<sub>10</sub>, from

which lattice parameter 'a' can be calculated. Lattice parameter 'a' gives the intercolumnar distance, which was found to be 49.9 Å.

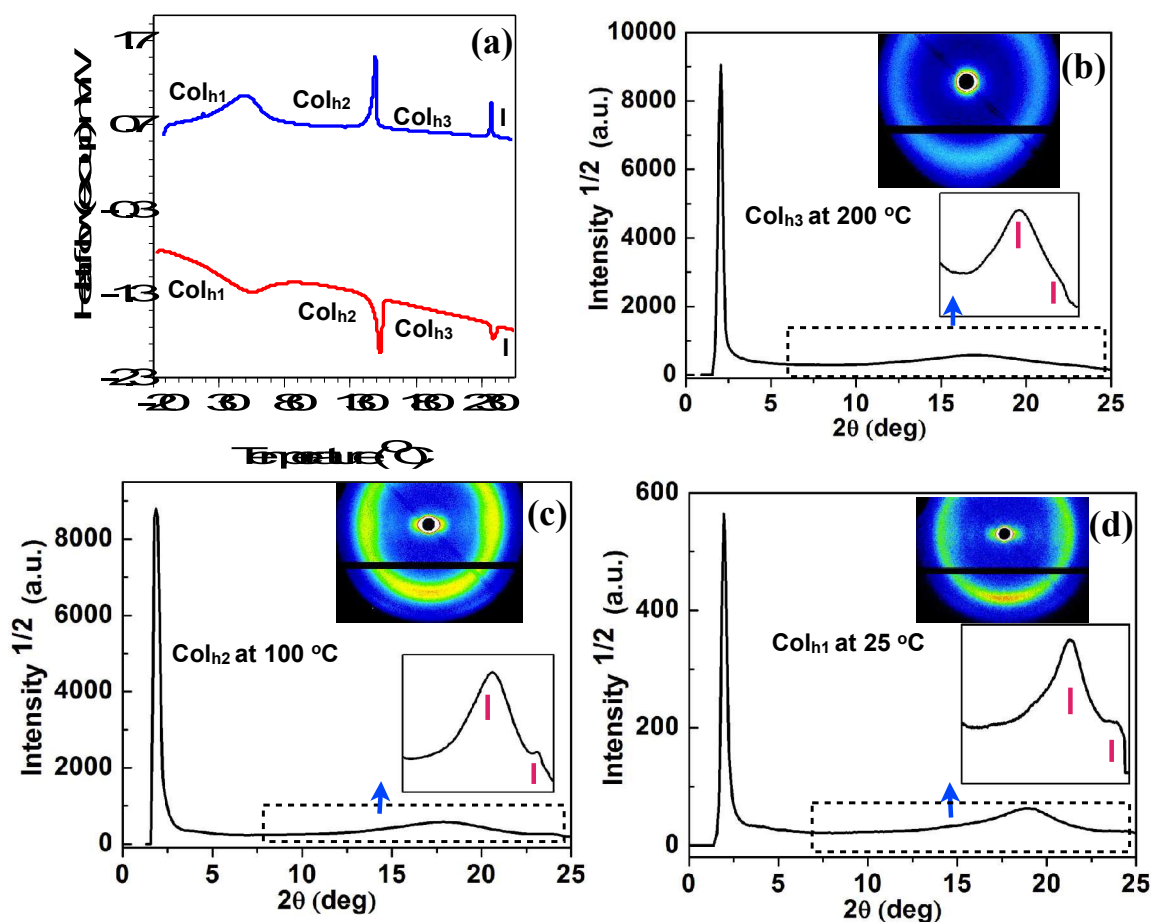


**Figure 3.** DSC traces obtained for first cooling (blue trace) and second heating (red trace) cycles of compound **1b** at a rate of 5 °C/min (a). XRD profiles depicting the intensity against the  $2\theta$  obtained for the Col<sub>h3</sub> phase of compound **1b** at 200 °C (b); Col<sub>h2</sub> phase of compound **1b** at 100 °C (c) and Col<sub>h1</sub> phase of compound **1b** at 25 °C; inset shows the image pattern obtained (d).

This is significantly lesser (25 %) than the molecular diameter, *i.e.* 65.78 Å, which may be due to the intercalation of peripheral flexible chains. This is understandable considering the large voids present between the arms of the star shaped molecule, where there is a possibility of alkyl chains filling up the voids (Fig. 4). The first diffused peak at 5.18 Å in wide-angle region corresponds to the packing of peripheral flexible tails, while the second diffused peak at 3.76 Å corresponds to the stacking of molecules in the individual columns (Fig. 3b). Similar intracolumnar distances are found in triindole-based discotics (3.9-4.4 Å), where the authors ascribed this due to the presence of phenyl linkers between the central core and peripheral flexible chains.<sup>27</sup> It is possible

that with the increase in the length of the arms in hekates, the arms are twisted in conformation with respect to the central planar core and this leads to an increase in the core-core stacking distance. Additionally these three different arms may have different diastereomeric

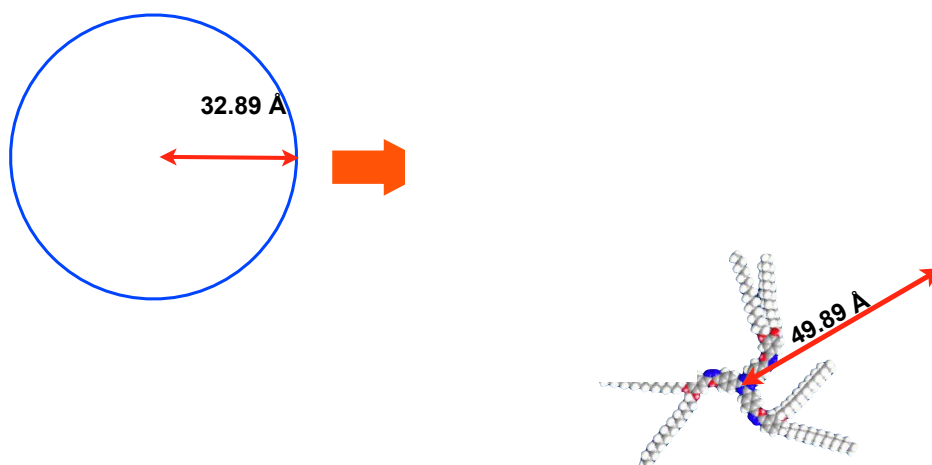


**Figure 4.** Schematic showing the self-assembly of compound **1b** into  $\text{Col}_h$  phase

conformations too. The small textural change observed at 149 °C along with the exothermic peak ( $\Delta H = 80.2$  kJ/mol) in DSC prompted us to carry out XRD studies well below this transition temperature, *i.e.* at 100 °C. The XRD pattern showed a single peak at low angle centered at 45.37 Å, along with the two diffused peaks at 4.96 Å and 3.76 Å. This diffraction pattern is similar to the high temperature  $\text{Col}_h$  phase observed for compound **1b**. The intercolumnar distance was found to be 52.4 Å. The intercolumnar distance 'a' is more than the observed intercolumnar distance at 200 °C (20 % lesser than molecular diameter). Thus the transition at 153 °C points to a transition between two  $\text{Col}_h$  phases. Such transition between two  $\text{Col}_h$  phases is not very common, but has been reported in literature.<sup>28</sup> As the intracolumnar distance remains constant at both temperatures, we observe only an increase in the intercolumnar distance by 5 Å. This may be due to the stretching of peripheral alkyl tails. Considering the transition at 50 °C with the unchanged texture we measured the XRD well below this temperature, *i.e.* at room temperature. The XRD pattern was almost similar to the measurement carried out at 100 °C, with the

comparable intercolumnar distance. The only difference was the decrease in alkyl chain stacking and core-core stacking distance. Thus compound **1b** exhibited a transition between three columnar hexagonal phases (designated as Col<sub>h1</sub>, Col<sub>h2</sub> and Col<sub>h3</sub>), as evidenced from POM, DSC and XRD studies. The difference between these three Col<sub>h</sub> phases is very subtle as seen from XRD studies. As you see in the table 2, for other compounds (**1c-d**), there was no significant change in intercolumnar distance with respect to temperature, which is very hard to explain. However we can infer from the data obtained that, compound **1b** with peripheral chains substituted at 3 and 4 positions of the benzene ring self-assemble with more intercalation at higher temperature Col<sub>h3</sub> phase than in low temperature Col<sub>h2</sub> and Col<sub>h1</sub> phase. There is also possibility that it can achieve various conformations due to its unsymmetrical peripheral substitution, which may be a reason for this observation. The decrease in the *d*-spacing values at wide-angle region with the decrease in temperature follows the usual trend. This difference between compound **1b** and **1c-d** is again due to the peripheral substitution.

Compound **1c**, which is a regioisomer of compound **1b** with six hexadecyloxy tails, exhibited wide range enantiotropic columnar mesophase over 150 degrees including room temperature. This is quite interesting to see how a small change in the substitution pattern, *i.e.* transition from peripheral 3,4- to 3,5-alkoxyl group substitution improves the mesophase stability of the star shaped molecules. The texture was a combination of mosaics, small focal conics and homeotropic regions and it remained unchanged at room temperature (Fig. 5a).

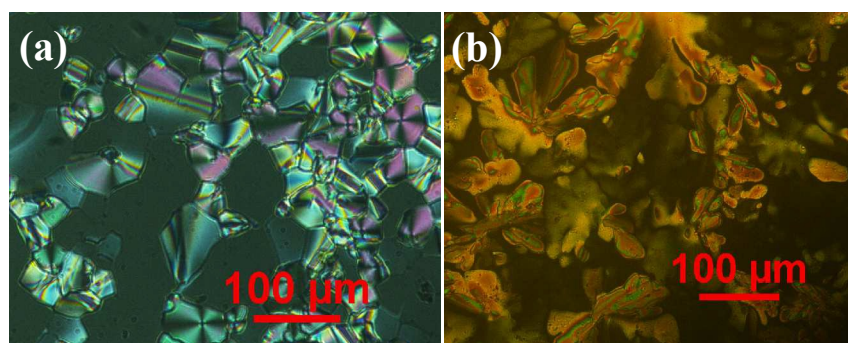


**Figure 5.** Photomicrographs of textures as seen by POM for the Col<sub>h</sub> phase of (a) compound **1c** at 30 °C and (b) compound **1d** at 237 °C.

Compound **1c**, in the cooling cycle of DSC thermogram showed a peak centered at 3 °C ( $\Delta H = 173.7$  kJ/mol) (see SI). Powder XRD studies conducted at different temperature intervals suggested that the phase under investigation is Col<sub>h</sub> as explained below. The powder XRD patterns at different temperatures showed a single reflection corresponding to Miller indices 100

(Fig.6a-c). The intercolumnar distance with the decrease in temperature showed little variation in contrast to the  $\text{Col}_h$  phase exhibited by compound **1b**, but higher interdigitation of peripheral alkyl tails.

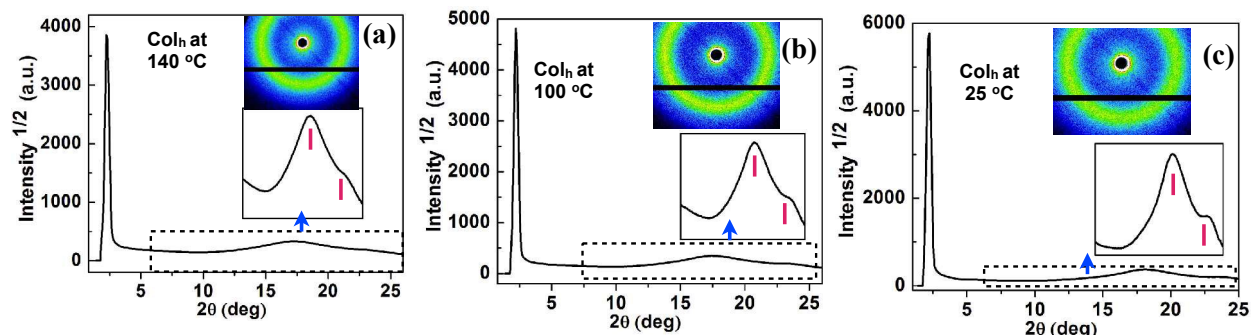


**Figure 6.** XRD profiles depicting the intensity against the  $2\theta$  obtained for the  $\text{Col}_h$  phase of compound **1c** at 140 °C (a);  $\text{Col}_h$  phase of compound **1c** at 100 °C (b) and  $\text{Col}_h$  phase of compound **1c** at 25 °C; inset shows the image pattern obtained.

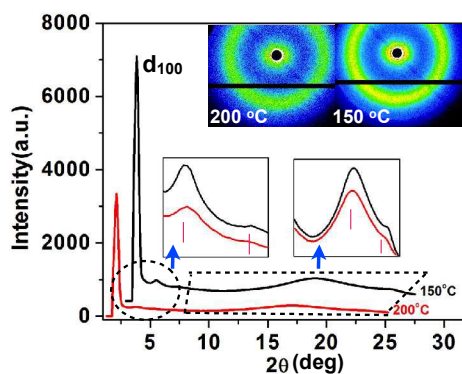


**Figure 7.** XRD profiles depicting the intensity against the  $2\theta$  obtained for the  $\text{Col}_h$  phase of compound **1d** at 200 °C (red trace) and at 150 °C (black trace) (inset shows the image pattern obtained).

Compound **1d**, with nine peripheral hexadecyloxy tails also exhibited wide range columnar hexagonal mesophase (Fig. 5b) of almost 200 degrees, with higher melting and isotropic temperatures in comparison to compound **1c**, which is confirmed by POM, DSC and XRD investigations. The powder XRD patterns recorded at 200 °C and 150 °C (Table 2, Fig.7) showed reflections at low angle corresponding to Miller indices 100, 110 and 210 with  $d$  spacing ratio of 1:0.57:0.38, which is fitting well with hexagonal lattice. Thus all the molecules except compound **1a** stabilized  $\text{Col}_h$  phase irrespective of the peripheral substitution. The lattice parameter of the  $\text{Col}_h$  phase ' $a$ ' is seemingly a constant with respect to temperature, which

implies to a small molecular rearrangement within the columns that is occurring due to the rearrangement of the alkyl chains.

We were curious to know the impact of shortening the length of peripheral alkyl chain on the thermal behavior of the star shaped molecules as in **2a-d** in comparison to compounds **1a-d**. Compounds **2a-d** are the lower homologues of compounds **1a-d** with *n*-dodecyloxy chains at the periphery, prepared by maintaining the same substitution pattern. Compound **2a** with three *n*-dodecyloxy chains was crystalline, but with a lower isotropic temperature than its higher homologue **1a**. Compound **2b** with six *n*-dodecyloxy chains exhibited an enantiotropic behavior with a higher isotropic temperature than compound **1b** and hence showing a larger mesophase width. The compound **2b** on cooling from the isotropic liquid state showed a birefringent pattern of mosaic texture (Fig. 8a), which is frequently observed for Col<sub>h</sub> phases. DSC scans in cooling cycle showed a transition at  $\approx 148$  °C ( $\Delta H = 60$  kJ/mol) (Fig. S57, Table 1), while texture did not show much variation except the change in color of the mosaic pattern, which remained unchanged till room temperature (Fig. 8b). The texture is not shearable, thus confirming the freezing of Col<sub>h</sub> phase in glassy state. But the second heating showed a crystallization peak at  $\approx 49$  °C ( $\Delta H = 225$  kJ/mol), before converting to form a birefringent fluidic pattern. XRD studies have been carried out at 220 °C, 130 °C and 25 °C. The XRD patterns were characteristic of Col<sub>h</sub> phase (Table 3, Fig. S58). The peaks at low angle can be indexed into Miller indices 100 and 200. These values are in the ratio of 1:1/ $\sqrt{4}$  conforming the hexagonal lattice (except the missing 1/ $\sqrt{3}$  reflection), which is similar to the XRD pattern observed for compound **1b**.

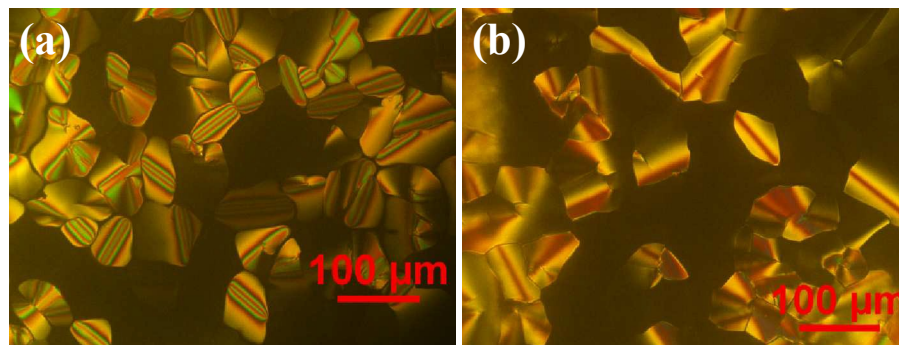


**Figure 8.** POM images obtained for the Col<sub>h</sub> phase of compound **2b** at 238 °C (a) and at room temperature (b).

The compound **2c** exhibited higher melting and isotropic temperatures than compound **1c**, which may be due to the increased core-core interaction and decreased fluidity of the molecular

structure. On cooling from the isotropic liquid the compound exhibited a mosaic texture interspersed with homeotropic domains. This optical texture showed a small change in the color and brightness at a temperature of 165 °C (Fig.9a and b), while there was no corresponding signature in DSC scans (Fig.9e). Further cooling showed a transition at  $\approx 85$  °C ( $\Delta H = 25.3$  kJ/mol), but the change in texture was minimal. Powder XRD studies carried out at 175 °C, 100 °C and at room temperature to investigate these observations (Fig.9f and Table 3). The XRD pattern obtained at 175 °C was reminiscent of Col<sub>h</sub> phase. The pattern consisted of three reflections at low angle corresponding to the  $d$  spacings of 41.48 Å, 23.29 Å and 15.79 Å, which can be indexed to 100, 110 and 210 reflections with a reciprocal spacing ratio of 1:1/ $\sqrt{3}$ :1/ $\sqrt{7}$ . This was accompanied with the two diffused peaks at the wide-angle region at  $d$  spacings of 5.25 Å and 3.76 Å, which correspond, to the packing of flexible tails and the rigid cores in the Col<sub>h</sub> phase. The diffraction pattern observed at 100 °C showed many peaks at low angle region. The five  $d$  spacings in the low angle region can be assigned to (110), (200), (220), (030) and (400) reflections from a rectangular lattice. The lattice constants were found to be  $a = 61.62$  Å and  $b =$

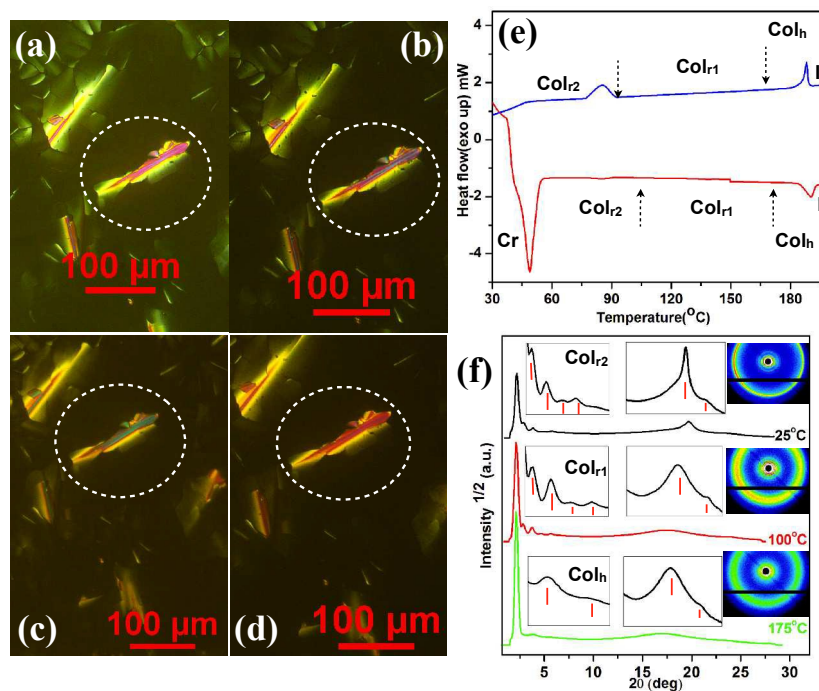


**Figure 9.** POM images of compound **2c** in Col<sub>h</sub> phase at 175 °C (a); Col<sub>h</sub> to Col<sub>r1</sub> transition at 165 °C (b); Col<sub>r1</sub> phase at 100 °C (c); Col<sub>r2</sub> phase at 25 °C (d); DSC scans for the first cooling (blue trace) and second heating (red trace) cycles (e); XRD profiles depicting the intensity against the  $2\theta$  obtained for the Col<sub>h</sub> phase of compound **2c** at 175 °C, Col<sub>r1</sub> phase at 100 °C and Col<sub>r2</sub> phase at 25 °C (f).

**Table 3.** Results of (*hkl*) indexation of XRD profiles of the compounds at a given temperature (T) of mesophase

Compounds (D/Å)	Phase (T/°C)	$d_{\text{obs}}(\text{Å})$	$d_{\text{cal}}(\text{Å})$	Miller indices <i>hkl</i>	Lattice parameter (Å)
<b>2b</b>	Col <sub>h2</sub> (220)	42.97 5.22( $h_a$ ) 3.75( $h_c$ )	42.94	100 001	$a = 49.59$
	Col <sub>h2</sub> (130)	45.67 22.53 5.01( $h_a$ ) 3.76( $h_c$ )	45.64 22.82	100 200 001	$a = 52.70$
	Col <sub>h1</sub> (25)	46.78 23.27 16.64 9.11 4.65( $h_a$ ) 3.72( $h_c$ )	46.75 23.38 17.67	100 200 210 001	$a = 53.98$
<b>2c</b>	Col <sub>h</sub> (175)	41.48 23.29 15.79 5.25( $h_a$ ) 3.76( $h_c$ )	41.46 23.94 15.67	100 110 210 001	$a = 47.87$
	Col <sub>r2</sub> (100)	41.47 30.81 23.67 18.88 15.47 5.10( $h_a$ ) 3.73( $h_c$ )	41.46 30.81 20.73 18.68 15.40	110 200 220 030 400 001	$a = 61.62$ $b = 56.06$
	Col <sub>r1</sub> (25)	39.73 30.75 23.06 18.13 15.21 12.26 4.50( $h_a$ ) 3.71( $h_c$ )	39.72 30.75 26.47 17.34 15.37 12.3	110 200 210 030 400 500 001	$a = 61.5$ $b = 52.04$
<b>2d</b>	Col <sub>h</sub> (230)	41.50 22.81 15.61 5.31( $h_a$ ) 3.83( $h_c$ )	41.47 23.94 15.68	100 110 210 001	$a = 47.89$
	Col <sub>h</sub> (150)	41.48 23.56 15.77 5.16( $h_a$ ) 3.75( $h_c$ )	41.46 23.94 15.67	100 110 210 001	$a = 47.87$
	Col <sub>r</sub> (25)	41.47 31.77 23.14 18.33 15.64 12.45 4.54( $h_a$ ) 3.71( $h_c$ )	41.46 31.77 20.73 18.24 15.88 12.70	110 200 220 030 400 500 001	$a = 63.54$ $b = 54.73$

56.06 Å. Formation of Col<sub>r</sub> phase requires higher core-core interaction as the first column should know how the neighboring column will organize. It is often found that in a series of compounds the compounds with shorter chains exhibit Col<sub>r</sub> phase.<sup>29, 1b, 1d</sup> In case of a columnar hexagonal to rectangular transition the (100) splits into two peaks mainly (110) and (200). This is because as soon as the lattice deviates from the hexagonal symmetry the  $d_{110}$  and  $d_{200}$  spacing no longer remains degenerate and two separate reflections are observed in the small angle region.<sup>1b</sup> The diffused peaks at wide-angle region with the  $d$  spacings 5.1 Å and 3.73 Å correspond to the packing of alkyl tails and the stacking of the aromatic cores. The room temperature XRD pattern also showed the similar diffraction pattern that can be assigned to Col<sub>r</sub> phase. Since there was an enthalpy change detected in DSC along with textural variation we have denoted these phases as Col<sub>r1</sub> and Col<sub>r2</sub>.

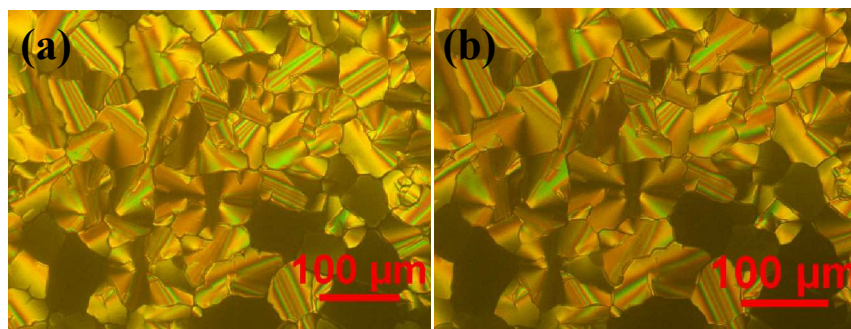


**Figure 10.** POM images of compound **2d** in Col<sub>h</sub> phase at 130 °C (a); and in Col<sub>r</sub> phase at room temperature (b).

Compound **2d** exhibited an improved thermal behavior in comparison to compound **1d**, but exhibited a transition between wide range Col<sub>h</sub> phase and Col<sub>r</sub> phase. Again the optical texture did not show much variation during this transition (Fig.10), but DSC scans showed the enthalpy change corresponding to this phase transition, which was further corroborated by XRD studies carried out at three different temperatures (Table 3, Fig. S58).

Thus the effect of lowering of chain length in these star shaped compounds from *n*-hexadecyloxy to *n*-dodecyloxy can be summarized as below. The thermal behavior of the compounds with three alkyl tails (**1a** and **2a**) was similar as they turned out to be crystalline irrespective of the chain length. The compounds with six alkyl tails (**1b** and **2b**), where the alkoxy groups are in adjacent position exhibited Col<sub>h</sub> phase. The lower chain analogue **2b** exhibited slightly enhanced thermal range. These two compounds show transitions between three

Col<sub>h</sub> phases, where the decrease in temperature led to Col<sub>h</sub> phase with shorter core-core distance and longer intercolumnar distance. The transition between different Col<sub>h</sub> phases may be due to the possibilities of attaining various conformations with respect to temperature, due to the unsymmetric peripheral substitution. This observation is limited to the type of peripheral substitution, which is not seen in the other compounds of the respective series. A marked difference was visible in the case of compounds **1c** and **2c**, where the alkyl tails are in alternate position. Compound **1c** exclusively stabilized Col<sub>h</sub> phase, while **2c** was bimesomorphic exhibiting high temperature Col<sub>h</sub> and low temperature Col<sub>r</sub> phases with enhanced thermal range. Similar behavior was observed in the case of compounds with nine alkoxy tails, *i.e.* compound **1d** and **2d**. Overall, the lowering of chain length has increased the core-core interaction, leading to stabilization of the Col<sub>r</sub> phase along with Col<sub>h</sub> phase and enhanced the thermal range. This demonstrated how a subtle change in the molecular structure through peripheral substitution alters the liquid crystal self-assembly.

Overall, these star shaped compounds showed enhanced mesophase stability in comparison to the earlier reported triazine based polyether derivatives, which showed Col phase only on complexation with trinitrofluorenone (TNF).<sup>29</sup> When compared to the similar star shaped mesogens containing tolane moieties which exhibit short range disordered Col<sub>h</sub> phases, present series of compounds exhibit ordered Col<sub>h</sub> phase over a wide thermal range, which may be due to the enhanced core-core interaction caused by the polar oxadiazole units.<sup>13</sup>

### Photophysical properties

We expected an influence on photophysical properties based on the substitution pattern but not on the length of the peripheral chain.<sup>26h</sup> The photophysical properties of the star shaped molecules **1a-d** and **2a-d** were studied in detail, *i.e.* in solution and thin film (Table 4). Absorption and fluorescence spectra of the compounds **1a-d** and **2a-d** were taken in micromolar THF solution (Fig. 11, Fig. S62). As can be seen, the absorption spectra for the solutions of compounds **1a-d** showed two absorption maxima in a range of 275-343 nm, while that of compound **2a-d** showed two absorption maxima in a range of 279-349 nm. These compounds showed large values of molar extinction coefficients ( $\epsilon = 16,610-28,490 \text{ M}^{-1} \text{ cm}^{-1}$ ). The absorption bands are corresponding to  $\pi-\pi^*$  and  $n-\pi^*$  transition of this molecular system. The first band at lower wavelength comes from 1,3,5-triazine system according to the previous

reports.<sup>13</sup> Optical bandgaps of these systems were calculated from the long edge of the absorption spectrum and found to fall in the range of 3.12-3.36eV.

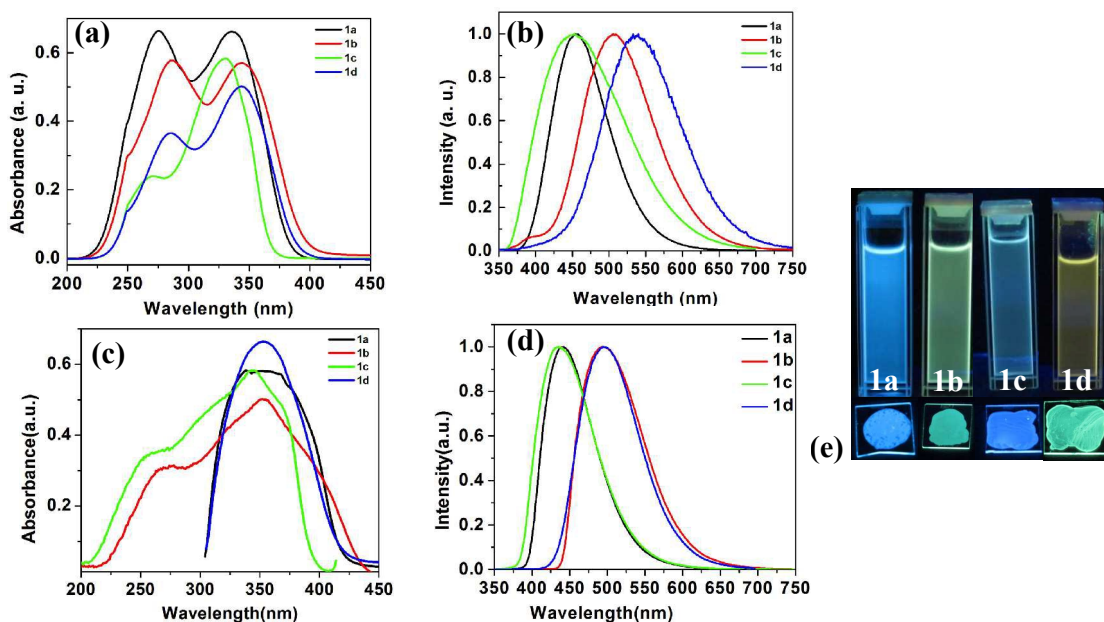


**Figure 11.** Absorption (a) and normalized emission spectra (b) in THF solution (20  $\mu$ M) obtained for **1a-d**; absorption (c) and normalized emission spectra (d) in thin film state; Pictures of solutions of compounds **1a-d** in THF and in thin film state (drop casted from 2 mM solutions in toluene) as seen with the illumination of 365 nm UV light (e).

Emission spectra of compounds **1a-d** and **2a-d** exhibited a single emission maximum centered around 453-540 nm with large Stoke's shift of 123-197 nm. Emission spectra changed with respect to substitution pattern at the periphery but not on the length of the peripheral tails (Fig. S62). Compounds **1a** and **1c** showed emission maxima centered at 458 and 453 nm with a blue emission in solution (at 365 nm UV light, Fig. 11e). Compounds **1b** and **1d** showed emission maxima centered at 506 and 540 nm with a green and yellow-green emission (at 365 nm UV light, Fig. 5e). Similar emission behavior was observed for compounds **2a-d** (Fig. S62). Relative quantum yields were measured with respect to quinine sulphate solution (0.1 M H<sub>2</sub>SO<sub>4</sub> with a quantum yield of 0.54) and found to be in the range of 0.28-0.33 (Table 4, Fig. S59). Steady state anisotropy values were in the range of 0.035-0.086. Thin films of the samples were produced by drop casting the 2 millimolar solutions of compounds in toluene on glass slides. The absorption spectra of these films were found to be broad, comprising single or two bands with a small red shift (Table 4, Fig. 11c, Fig. S62), while the emission spectra did not vary much from the

**Table 4.** Photophysical properties of compounds **1a-d** in solution<sup>a</sup> and film state

Entry	Solution State							Thin film State		
	Absorption (nm)	Emission <sup>b</sup> (nm)	Stokes shift (nm)	$\lambda_{\text{onset}}$ (nm)	$\Delta E_{\text{g, opt}}^{\text{c,d}}$	Steady state anisotropy	Relative Quantum Yield	Absorption (nm)	Emission <sup>b</sup> (nm)	Stokes shift (nm)
<b>1a</b>	275,335	458	123	386	3.21	0.067	0.28	356	442	86
<b>1b</b>	286,343	506	163	397	3.12	0.083	0.31	276, 352	495	143
<b>1c</b>	285,331	453	122	369	3.36	0.070	0.29	262, 345	435	90
<b>1d</b>	271,343	540	197	395	3.14	0.086	0.31	352	495	143
<b>2a</b>	279, 340	456	116	387	3.21	0.054	0.25	349	455	107
<b>2b</b>	279, 349	501	152	394	3.15	0.035	0.33	263, 354	487	133
<b>2c</b>	270, 329	451	122	366	3.39	0.045	0.27	267, 346	449	105
<b>2d</b>	283, 344	537	193	385	3.23	0.053	0.31	357	504	147

<sup>a</sup>micromolar solutions in THF; <sup>b</sup>excited at the respective absorption maxima; <sup>c</sup>Band gap determined from the red edge of the longest wave length ( $\lambda_{\text{onset}}$ ) in the UV-vis absorption spectra; <sup>d</sup> In volts (eV).

solution spectra, but they showed a blue shift. In the case of compounds **1a** and **1b** the observed blue shift was 16 nm and 11 nm respectively, while in the case of compounds **1c** and **1d** the blue shift was found to be 18 nm and 45 nm respectively. Similar behavior was observed in the case of compounds **2a-d** (Fig. S62). Further if we look closely at the absorption spectra of these compounds in thin film state, we see that there is a band at lower wavelength observed only for compounds **1b**, **1c**, **2b** and **2c**. This is observed specifically to these compounds, which contain six alkyl tails, confirming that this is arising because of the solid-state packing that is different from compounds **1a**, **1d**, **2a** and **2d**. The emission colors observed under the long wavelength UV light was almost similar to that obtained in solutions (Fig. 11e). Red shifted absorption bands in the solid state, is usually observed with the formation of J-aggregates; where the molecules are stacked in a head to tail fashion,<sup>30</sup> but we can not rule out this observation due to the organization of the star shaped molecules in different diastereomeric conformations within the column.

In order to get a clear view of the aggregation phenomena we have measured the UV and fluorescence spectra of these compounds as a function of increasing concentration starting from micromolar solution in THF. At a particular concentration ( $6.25 \times 10^{-5}$  M for compounds **1a-c**,  $3.12 \times 10^{-5}$  M for compound **1d**) the luminescence intensity was found to be high (Figure 12a). Further increase in concentration reduced the luminescence intensity, which may be due to the aggregation induced quenching. We have measured the fluorescence lifetime at three different concentrations to understand this observation. Fluorescence lifetime measurements at

micromolar concentrations revealed the existence of one species, which is solvated monomer. At a concentration where the luminescence intensity was high, we observed two species, one with lower lifetime and the other with higher lifetime. This biexponential decay is due to the presence of aggregated species and solvated monomers. The presence of two species is may be due to the high solubility of these compounds in THF. Some of the molecules may prefer to remain as solvated monomers even at highest concentration (Fig. S63 and Table 1 in SI). The absorption spectra showed two maxima where the first one at lower wavelength was found with reduced intensity in comparison to the absorption spectra obtained for micromolar solution (Fig.12b). All the compounds except compound **1c** showed a small red shift in their absorption maximum, while the absorption maximum of **1c** did not change much (Table 4 and 5). Similarly the

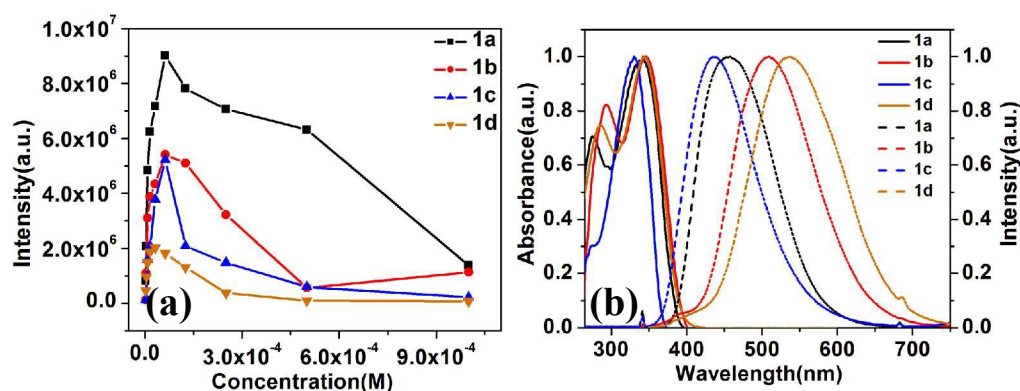


**Figure 12.** (a) Emission intensity vs concentration plots of compounds **1a-d** in THF solution (a); Absorption and emission spectra at the concentration where highest emission intensity was observed (b).

**Table 5.** Photophysical properties of compounds **1a-c** ( $6.25 \times 10^{-5}$ M) and **1d** ( $3.12 \times 10^{-5}$ M) in THF solution and in thin film drop casted from 2 mM solutions in toluene

Entry	Absorption (nm)	Emission (nm)	Fraction of molecules	Life time (ns)	Absorption (nm)	Emission (nm)	Fraction of molecules	Life time (ns)
<b>1a</b>	275, 338	452	65%, 35%	3.50, 1.67	356	442	86%, 14%	3.64, 0.72
<b>1b</b>	293, 346	510	53%, 47%	13.40, 3.01	276, 352	495	50%, 50%	10.19, 2.55
<b>1c</b>	274, 331	435	53%, 47%	6.24, 0.82	262, 345	435	51%, 49%	10.83, 2.11
<b>1d</b>	286, 344	535	49%, 51%	3.79, 0.93	352	495	74%, 26%	8.65, 2.81

luminescence spectra showed a blue shifted emission maximum for all the compounds except compound **1b**, which showed a small red shift. Thus as we see from Tables 4 and 5, absorption and emission spectra follow a similar trend (either gradual decrease or increase in the wavelength) as they move from low to high concentration or to thin film state. The fluorescence

lifetime measurements carried out for the thin films showed two life times, one is of higher lifetime corresponding to aggregates, while the lower one is corresponding to monomer species. The data is comparable to the properties of these compounds in solution state (Table 5).

We were particularly interested to examine the photophysical properties of compound **1c** and **2c**, which exhibit room temperature Col<sub>h</sub> and Col<sub>r</sub> phase respectively. A thin film of compound **1c** was prepared by heating the sample sandwiched between two glass slides to isotropic state and annealing it to room temperature. Similarly a thin film of compound **2c** was prepared by annealing it in Col<sub>r</sub> phase. The liquid crystal film of compound **1c** showed an absorption maximum of 347 nm, which is red shifted by 16 nm in comparison to solution spectra. Emission spectrum was blue shifted with an emission maximum of 435 nm (Stoke's shift  $\approx$  90 nm) (Fig. 13a). This observation was in line with the data obtained for the drop casted samples.

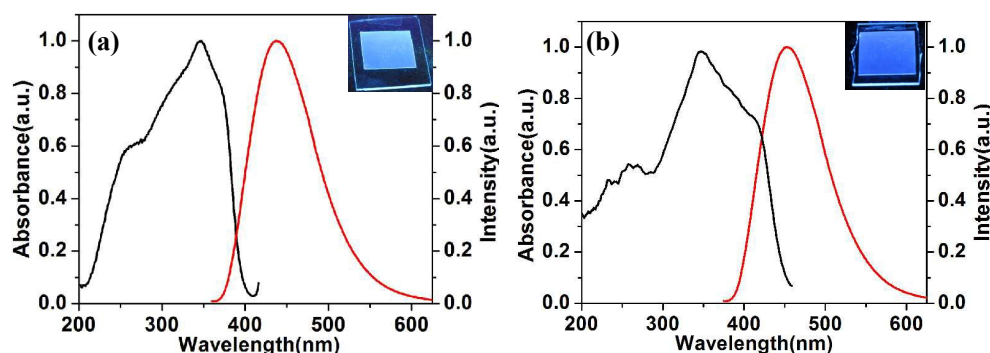


**Figure 13.** (a) Normalized absorption (black trace) and emission spectra (red trace) of LC thin film of compound **1c** (inset shows the thin film under UV light) (a) and for compound **2c** (b).

In literature, observation of red-shifted absorption maximum in comparison to that in solution state is attributed to the formation of J-type aggregates.<sup>31</sup> But considering the possibilities of various diastereomeric conformations that can be attained by these molecules, we cannot specify this observation to the formation of J-type aggregates. The absorption spectra of compound **2c** were also red-shifted in comparison to the solution spectra by 16 nm (absorption maximum: 349 nm), while there was no much difference with respect to the emission spectra (emission maximum: 452 nm). This behavior is similar to that of compound **1c** irrespective of the chain length and type of columnar packing. Similar star shaped compounds reported by others, where a central triazine core connected with *trans*-stilbene chromophores showed a blue shifted emission,<sup>12b</sup> while the molecules with tolane moieties showed red shifted

emission.<sup>13a</sup> Preservation of solid-state/liquid crystal state emission along with good thermal stability make these compounds promising for organic dye lasers and OLEDs.

#### IV. Electrochemical properties

Energy levels of frontier molecular orbitals (HOMO and LUMO) and the energy gap of these levels in star shaped molecules **1a-d** were obtained by cyclic voltammetry (CV) and the data are tabulated in Table 6. All the compounds exhibited irreversible oxidation and reduction waves (See SI). The optical band gap  $E_{g,opt}$  was estimated from the red edge of the absorption spectra. Energy levels of LUMO and HOMO were determined by using the formulae  $E_{LUMO} = -(4.8 - E_{1/2, Fc, Fc^{+}} + E_{red, onset})$  eV,  $E_{HOMO} = -(4.8 - E_{1/2, Fc, Fc^{+}} + E_{ox, onset})$  eV. There was no much impact on the energy levels of frontier molecular orbitals with respect to substitution, and the bandgaps were found to be in the range of 2.53-2.62 eV. These values are slightly smaller than their corresponding optical band gap values (Table 4).

**Table 6.** Electrochemical properties of compounds **1a-d** in micromolar dichloromethane solutions

Entry	$E_{Ired}$	$E_{Ioxd}$	$E_{HOMO}$	$E_{LUMO}$	$\Delta E_{CV}$	$\Delta E_{g, opt}$
<b>1a</b>	-1.02 V	1.57 V	-5.91eV	-3.32eV	2.59eV	3.21eV
<b>1b</b>	-1.05 V	1.48 V	-5.82eV	-3.29eV	2.53eV	3.12eV
<b>1c</b>	-1.11 V	1.48 V	-5.82eV	-3.23eV	2.59eV	3.36eV
<b>1d</b>	-1.03 V	1.59 V	-5.93eV	-3.31eV	2.62eV	3.14eV

These values can be compared with 2,4,6-triphenyl-1,3,5-triazine, which is one of the oldest materials used in OLED fabrication as a hole-blocking material.<sup>32</sup> This compound exhibits a LUMO and HOMO levels of -2.8 eV and -6.5 eV respectively. The optical band gap was found to be 3.71eV,<sup>33</sup> which is higher than the present series where three symmetrically substituted 1,3,4-oxadiazoles are connected to the central ring (3.2-3.4 eV) (Table 4). The LUMO levels of the compounds **1a-d** were lower than 2,4,6-triphenyl-1,3,5-triazine (-3.23 to -3.32 eV), while the HOMO levels higher and were in the range of -5.8 to -5.9eV. Thus the substitution with alkoxyphenyl oxadiazole moiety on the 2,4,6-triphenyl-1,3,5-triazine lowers the LUMO; increases the HOMO level and thus a resultant lowering of the band gap. The lower LUMO level and bandgaps of these star-shaped molecules may reduce the barriers for electrons, with the simultaneous blocking of the hole movement. Thus the extensive  $\pi$ -conjugation and the introduction of the electron donating groups to the electron deficient central triazine ring is a

simple method to modify the frontier molecular orbital energy levels and band gap. Additionally the 1,3,4-oxadiazole units bring about the higher thermal stability and emissive nature that is very vital for the solid-state display devices. Similar comparable values were observed when the central triazine unit was connected to fluorene through different linkers.<sup>33,34</sup>

## V. Experimental Section

Commercially available chemicals were used without any purification; solvents were dried following the standard procedures. Chromatography was performed using either silica gel (60-120 and 100-200) or neutral aluminium oxide. For thin layer chromatography, aluminium sheets pre-coated with silica gel were employed. IR spectra were recorded on a Perkin Elmer IR spectrometer at normal temperature by using KBr pellet. The spectral positions are given in wave number ( $\text{cm}^{-1}$ ) unit. NMR spectra were recorded using Varian Mercury 400 MHz or Bruker 600 MHz NMR spectrometer (at 298K). For  $^1\text{H}$  NMR spectra, the chemical shifts are reported in ppm relative to TMS as an internal standard. Coupling constants are given in Hz. Mass spectra were obtained from MALDI-TOF mass spectrometer in Laser Desorption positive mode using  $\alpha$ -cyano-4-hydroxycinnamic acid matrix or from High Resolution Mass Spectrometer.

The mesogenic compounds were investigated for their liquid crystalline behavior by employing a polarizing optical microscope (POM) (Nikon Eclipse LV100POL) equipped with a programmable hot stage (Mettler Toledo FP90). Clean glass slides and coverslips were employed for the polarizing optical microscopic observations. The transition temperatures and associated enthalpy changes were determined by differential scanning calorimeter (Mettler Toledo DSC1) under nitrogen atmosphere. Peak temperatures obtained in DSC, corresponding to the phase transitions were in agreement with the POM observations. The transition temperatures obtained from calorimetric measurements of the second heating and first cooling cycles at a rate of  $5\text{ }^\circ\text{C}/\text{min}$  are tabulated. In the cases where the DSC signatures are not observed for the phase transitions, the transition temperatures have been taken from POM observations. Temperature dependent X-ray diffraction studies were carried on unaligned powder samples in Lindemann capillaries (1 mm diameter) held in programmable hot stage and irradiated with  $\text{CuK}\alpha$  radiation ( $\lambda = 1.5418\text{ \AA}$ ). The samples were filled in the capillary tube in their isotropic state and their both ends were flame sealed. The apparatus essentially consisted of a high-resolution powder X-ray

diffractometer (Xenocs) equipped with a focusing elliptical mirror and a high-resolution fast detector. Thermogravimetric analysis (TGA) was performed using thermogravimetric analyzer (Mettler Toledo, model TG/SDTA 851e) under constant nitrogen flow at a heating rate of 10 °C/min. UV-Vis spectra were obtained by using Perkin-Elmer Lambda 750, UV/VIS/NIR spectrometer. Fluorescence emission spectra in solution state were recorded with Horiba Fluoromax-4 fluorescence spectrophotometer or Perkin Elmer LS 50B spectrometer. Cyclic Voltammetry studies were carried out using a PAR Model 700D series Electrochemical workstation. Experiments were carried out in micromolar solutions in dichloromethane at room temperature and experiments were done at a scanning rate of 0.05 mV s<sup>-1</sup>. For the CV experiments Ag/AgNO<sub>3</sub> as the reference electrode, glassy carbon working electrode, platinum rod counter electrodes were used. Tetrabutyl ammonium perchlorate (0.1 M) was used as a supporting electrolyte. The half-wave potential of the ferrocene/ferrocenium (Fc/Fc<sup>+</sup>) redox couple ( $E_{1/2, \text{Fc, Fc}^+}$ ) was found to be 0.46 V relative to the Ag/Ag<sup>+</sup> reference electrode. HOMO energy levels were estimated from the onset oxidation peak values, by using the formula  $E_{\text{HOMO}} = -(4.8 - E_{1/2, \text{Fc, Fc}^+} + E_{\text{ox, onset}})$  eV, while LUMO energy levels were estimated from the onset reduction peak values by using  $E_{\text{LUMO}} = -(4.8 - E_{1/2, \text{Fc, Fc}^+} + E_{\text{red, onset}})$  eV. Electrochemical band gaps were estimated from the formula  $\Delta E_{\text{CV}} = (E_{\text{LUMO}} - E_{\text{HOMO}})$  eV, while optical band gaps were determined from the red edge of the longest wavelength in the UV-Vis absorption spectra. Time resolved fluorescence was measured using an Edinburgh Instruments Life Spec II instrument. Here the fluorescence lifetimes were determined by a time-correlated single photon counting method. A Hamamatsu micro channel plate (MCP) detector that has a response time of 50 ps was used in the abovementioned instrument. A picosecond 375 nm laser diode and 336 LED were used as the light sources. The full width at half maxima for the laser diode and the LED are 90 ps and 570 ps respectively. The fluorescence emission maxima for the corresponding species has been chosen as the monitoring wavelength in the time resolved fluorescence measurements. The data were analyzed using a reconvolution method using the software provided by Edinburgh instruments.

## VI. Summary

In summary, we have synthesized eight new star-shaped molecules with a central 2,4,6-triphenyl triazine core attached with three symmetrically substituted 1,3,4-oxadiazole arms with the variation in the number, length and pattern of peripheral chain substitution. These compounds

were investigated for their thermal, electrochemical and photophysical properties with the help of various techniques. Compound with three flexible chains at the periphery turned out to be crystalline irrespective of the chain length, whereas compounds with six and nine peripheral chains stabilized  $\text{Col}_h$  phase over a wide thermal range. One of the compounds with peripheral *n*-hexadecyloxy substitution at 3 and 4 positions showed a technologically important room temperature  $\text{Col}_h$  phase. Lowering of chain length in these star shaped compounds from *n*-hexadecyloxy to *n*-dodecyloxy enhanced the mesophase range. The compound with three alkyl tails was crystalline, while the compound with six alkyl tails, where the alkoxy groups are in adjacent position exhibited  $\text{Col}_h$  phase with a slight enhancement in the thermal range. A marked difference was visible in the case of compound, where the alkyl tails were in alternate position. This compound exhibited high temperature  $\text{Col}_h$  and low temperature  $\text{Col}_r$  phases with enhanced thermal range. Similar behavior was observed in the case of compounds with nine alkoxy tails. Overall, the lowering of chain length has increased the core-core interaction, leading to stabilization of the  $\text{Col}_r$  phase along with  $\text{Col}_h$  phase and enhanced the thermal range. This demonstrated how a subtle change in the molecular structure through peripheral substitution alters the liquid crystal self-assembly.

The photophysical properties of these star shaped molecules were extremely dependent on the number and pattern of peripheral chain substitution. They exhibited blue and green fluorescence in solid/liquid crystal state. Preserved fluorescence in the solid state is explained due to the formation of aggregates, which do not quench the fluorescence. The aggregation quenching is not occurring here probably due to the columnar packing that includes several different diastereomeric conformations. Cyclic voltammetry studies revealed that, these molecules possess lower LUMO levels and bandgaps compared to the 2,4,6-triphenyl triazine which is used in OLEDs, thus making them better candidates for electron transporting emissive layers. The ability to overcome the aggregation induced quenching of the fluorescence, higher thermal stability and beneficial band gap are the properties which make these molecules promising from the view point of emissive displays and organic lasers.

### VIII. Associated Content

The synthesis and characterization details,  $^1\text{H}$  NMR,  $^{13}\text{C}$  NMR spectra of all new compounds, absorption and emission spectra, POM photographs, DSC thermograms, XRD profiles of LC

compounds and Cyclic voltammograms are provided as electronic supporting information. This material is available free of charge via the Internet.

## Acknowledgements

ASA sincerely thanks Science and Engineering Board (SERB), DST, Govt. of India and Board of Research in Nuclear Sciences-Department of Atomic Energy (BRNS-DAE) for funding this work through the project No.SB/S1/PC-37/2012 and No. 2012/34/31/BRNS/1039 respectively. We thank Ministry of Human Resource Development for Centre of Excellence in FAST (F. No. 5-7/2014-TS-VII). ASA acknowledges Central Instrumentation Facility, IIT Guwahati for analytical facilities. We acknowledge Dr. Chandan Mukherjee, IIT Guwahati for providing his Electrochemical workstation.

## References

1. (a) R. J. Bushby and O. R. Lozman, *Current Opinion in Colloid & Interface Science*, 2002, **7**, 343-354; (b) S. Laschat, A. Baro, N. Steinke, F. Giesselmann, C. Hägele, G. Scalia, R. Judele, E. Kapatsina, S. Sauer, A. Schreivogel and M. Tosoni, *Angew. Chem. Int. Ed.*, 2007, **46**, 4832-4887; (c) S. Kumar, *Isr. J. Chem.*, 2012, **52**, 820-829; (d) T. Wöhrle, I. Wurzbach, J. Kirres, A. Kostidou, N. Kapernaum, J. Litterscheidt, J. C. Haenle, P. Staffeld, A. Baro, F. Giesselmann and S. Laschat, *Chem. Rev.*, 2015, DOI: 10.1021/acs.chemrev.5b00190
2. J. W. Goodby, P. J. Collings, T. Kato, C. Tschierske, H. Gleeson and P. Raynes, *Handbook of Liquid Crystals: Fundamentals* ed., Wiley-VCH, Weinheim, Germany, 2014, **1**.
3. M. Lehmann, *Chem. Eur. J.*, 2009, **15**, 3638-3651.
4. (a) H. Detert, M. Lehmann and H. Meier, *Materials*, 2010, **3**, 3218-3330; (b) B. Roy, N. De and K. C. Majumdar, *Chem. Eur. J.*, 2012, **18**, 14560-14588.
5. (a) G. H. Mehl, A. J. Thornton and J. W. Goodby, *Mol. Cryst. Liq. Cryst.*, 1999, **332**, 455 - 461; (b) D. Goldmann, D. Janietz, C. Schmidt and J. H. Wendorff, *Liq. Cryst.*, 1998, **25**, 711-719; (c) J. Barbera, L. Puig, P. Romero, J. L. Serrano, and T. Sierra, *J. Am. Chem. Soc.*, **2005**, 127, 458-464.
6. F. Yang, J. Xie, H. Guo, B. Xu and C. Li, *Liq. Cryst.*, 2012, **39**, 1368-1374.
7. (a) M. B. Steffensen, E. Hollink, F. Kuschel, M. Bauer and E. E. Simanek, *J. Polym. Sci., Part A: Polym. Chem.*, 2006, **44**, 3411; (b) L. L. Lai, C. H. Lee, L. Y. Wang, K. L. Cheng and H. F. Hsu, *J. Org. Chem.*, 2008, **73**, 485 - 490.
8. H. C. Jeong, M. J. Piao, S. H. Lee, M. Y. Jeong, K. M. Kang, G. Park, S. J. Jeon and B. R. Cho, *Adv. Funct. Mater.*, 2004, **14**, 64 - 70.
9. K. C. Majumdar, N. De, B. Roy and A. Bhaumik, *Liq. Cryst.*, 2010, **37**, 1459 - 1464.

10. (a) W. Shu and S. Valiyaveetil, *Chem. Commun.*, 2002, 1350 – 1351; (b) H. Lee, D. Kim, H. K. Lee, W. Qiu, N. K. Oh, W. C. Zin and K. Kim, *Tetrahedron Lett.*, 2004, **45**, 1019 – 1022.
11. S. Kotha, D. Kashinath and S. Kumar, *Tetrahedron Lett.*, 2008, **49**, 5419 – 5423.
12. (a) H. C. Holst, T. Pakula and H. Meier, *Tetrahedron*, 2004, **60**, 6765 – 6775; (b) H. K. Dambal and C. V. Yelamaggad, *Tetrahedron Lett.*, 2012, **53**, 186–190.
13. (a) C. H. Lee and T. Yamamoto, *Tetrahedron Lett.*, 2001, **42**, 3993 – 3996; (b) C. H. Lee and T. Yamamoto, *Bull. Chem. Soc. Jpn.*, 2002, **75**, 615–618.
14. R. Bai, S. Li, Y. Zou, C. Pan, P. Xie, B. Kong, X. Zhou and R. Zhang, *Liq. Cryst.*, 2001, **28**, 1873 – 1876.
15. (a) E. Beltran, J. L. Serrano, T. Sierra and R. Gimenez, *Org. Lett.*, 2010, **12**, 1404–1407; (b) E. Beltran, J. L. Serrano, T. Sierra and R. Gimenez, *J. Mater. Chem.*, 2012, **22**, 7797–7805.
16. T. Yasuda, T. Shimizu, F. Liu, G. Ungar and T. Kato, *J. Am. Chem. Soc.*, 2011, **133**, 13437 – 13444.
17. H. W. Gibson, D. L. Dotson, H. Marand and T. M. Swager, *Mol. Cry. Liq. Cry.*, 2006, **326**, 113 -138.
18. Y.-D. Zhang, K. G. Jespersen, M. Kempe, J. A. Kornfield, S. Barlow, B. Kippelen and S. R. Marder, *Langmuir*, 2003, **19**, 6534–6536.
19. (a) R. Cristiano, D. M. P. D. O. Santos and H. Gallardo, *Liq. Cryst.*, 2005, **32**, 7–14; (b) S. K. Pathak, R. K. Gupta, S. Nath, D. S. Shankar Rao, S. K. Prasad and A. S. Achalkumar, *J. Mater. Chem. C.*, 2015, **3**, 2940-2952.
20. H. Yu, B. Liu, Y. Wang, J. Wang and Q. Hao, *SoftMatter*, 2011, **7**, 5113–5115.
21. H. Dai, X. Yang, X. Tan, F. Su, X. Cheng, F. Liu and C. Tschierske, *Chem. Commun.*, 2013, **49**, 10617-10619
22. S. K. Pathak, R. K. Gupta, S. Nath, D. S. Shankar Rao, S. K. Prasad and A. S. Achalkumar, *J. Mater. Chem. C*, 2015, **3**, 8166-8182.
23. D. Sun, S. Ma, Y. Ke, D. J. Collins and H. C. Zhou, *J. Am. Chem. Soc.*, 2006, **128**, 3896-3897.
24. Z. Lin, T. J. Emge, R. Warmuth, *Chem. Eur. J.*, 2011, **17**, 9395 – 9405.
25. J. Barbera, M. A. Godoy, P. I. Hidalgo, M. L. Parra, J. A. Ulloa and J. M. Vergara, *Liq. Cryst.*, 2007, **34**, 1249–1267.
26. (a) J. Barbera, R. Gimenez and J. L. Serrano, *Chem. Mater.*, 2000, **12**, 481–489; (b) J. L. Serrano and T. Sierra, *Chem.–Eur. J.*, 2000, **6**, 759–766; (c) S. Ito, M. Ando, A. Nomura, N. Morita, C. Kabuto, H. Mukai, K. Ohta, J. Kawakami, A. Yoshizawa and A. Tajiri, *J. Org. Chem.*, 2005, **70**, 3939–3949; (e) A. Hayer, V. de Halleux, A. Kohler, A. El-Garouhy, E. W. Meijer, J. Barbera, J. Tant, J. Levin, M. Lehmann, J. Gierschner, J. Cornil and Y. H. Geerts, *J. Phys. Chem. B*, 2006, **110**, 7653–7659; (f) L. Alavarez, J. Barbera, L. Puig, P. Romero, J. L. Serrano and T. Sierra, *J. Mater. Chem.*, 2006, **16**, 3768–3773; (g) C. V. Yelamaggad, A. S. Achalkumar, D. S. S. Rao and S. K. Prasad, *J. Mater. Chem.*, 2007, **17**, 4521–4529; (h) C. V. Yelamaggad, A. S. Achalkumar, D. S. S. Rao and S. K. Prasad, *J. Org. Chem.*, 2007, **72**, 8308–8318; (i) C.

- V. Yelamaggad, A. S. Achalkumar, D. S. S. Rao, M. Nobusawa, H. Akutsu, J. Yamada and S. Nakatsuji, *J. Mater. Chem.*, 2008, **18**, 3433–3437; (j) A. S. Achalkumar, U. S. Hiremath, D. S. Shankar Rao, S. Krishna Prasad and C. V. Yelamaggad, *J. Org. Chem.*, 2013, **78**, 527–544.
27. E. M. García-Frutos, U. K. Pandey, R. Termine, A. Omenat, J. Barberá, J. L. Serrano, A. Golemme and B. Gómez-Lor, *Angew. Chem. Int. Ed.*, 2011, **50**, 7399–7402.
28. S. Ito, M. Ando, A. Nomura, N. Morita, C. Kabuto, H. Mukai, K. Ohta, J. Kawakami, A. Yoshizawa and A. Tajiri, *J. Org. Chem.*, 2005, **70**, 3939–3949.
29. C. V. Yelamaggad, A. S. Achalkumar, D. S. Shankar Rao, and S. Krishna Prasad, *J. Org. Chem.* **2007**, *72*, 8308-8318.
30. S. Kotha, D. Kashinath and S. Kumar, *Tetrahedron Lett.* 2008, **49**, 5419 – 5423.
31. F. Würthner, T. E. Kaiser and C. R. Saha-Möller, *Angew. Chem. Int. Ed.*, 2011, **50**, 3376–3410.
32. D. D. Prabhu, N. S. S. Kumar, A. P. Sivadas, S. Varghese and S. Das, *J. Phys. Chem. B*, 2012, **116**, 13071–13080.
33. R. Fink, C. Frenz, M. Thelakkat and H.-W. Schmidt, *Macromolecules*, 1997, **30**, 8177-8181.
34. H. Zhong, H. Lai, and Q. Fang, *J. Phys. Chem. C*, 2011, **115**, 2423–2427.
35. N. A. Kukhta, J. Simokaitiene, D. Volyniuk, J. Ostrauskaite, J. V. Grazulevicius, G. Juska and V. Jankauskas, *Synthetic Metals*, 2014, **195**, 266–275.